The experimentally observed emission in the parallel plane contains not only transition radiation but also the parallel component of bremsstrahlung. Therefore, the spectral distribution curves were analyzed initially by subtracting from the experimental intensity in the parallel plane $I_{\parallel}$, the quantity $(d\sigma_{\parallel}/d\sigma_{\perp})I_{\perp}$ where $(d\sigma_{\parallel}/d\sigma_{\perp})$ is the ratio of the parallel to perpendicular yield calculated by Gluckstern, Hull, and Breit[10] and given by the inverse of Eq. (4), and the quantity $I_{\perp}$ is the intensity observed experimentally in the perpendicular plane. An analysis of the data in this fashion showed a little better agreement. However, better agreement still was obtained by letting the ratio $(d\sigma_{\parallel}/d\sigma_{\perp})$ be equal to 1 as shown by the dashed curves in Figs. 1 and 2. Whereas before, agreement between theory and experiment was obtained only for the higher energies, now agreement is good for all beam energies. The interpretation of the data in this fashion suggests that the observed bremsstrahlung is unpolarized. The calculations of Gluckstern, Hull, and Breit[10] for isolated atoms show that the ratio $(d\sigma_{\parallel}/d\sigma_{\perp})$ is approximately 0.5. The inclusion of optical effects will increase this ratio because light transmitted through a dielectric medium is preferentially polarized in the plane of incidence. This effect will raise the intensity in the parallel plane and, thus, the ratio $(d\sigma_{\parallel}/d\sigma_{\perp})$ will be greater than 0.5 and might easily be of the order of unity as found experimentally.

PHYSICAL REVIEW VOLUME 131, NUMBER 2 15 JULY 1963

Fission Fragment Angular Distributions and Cross Sections for Deuteron-Induced Fission*

GEORGE L. BATE,† R. CHAUDHRY,‡ AND J. R. HUIZENGA
Argonne National Laboratory, Argonne, Illinois
(Received 15 February 1963)

Fission-fragment angular distributions and cross sections have been measured with gold surface barrier semiconductor detectors for fission induced in a group of elements from Tl to Pu by deuterons of 7- to 21-MeV energy. Apart from a pronounced dip in the radium region, the differential fission fragment cross-section ratios $W(174°)/W(90°)$ at 21 MeV show an increasing trend with decreasing Z^2/A, the values ranging from 1.20 for Pu^{239} to 1.58 for natural Tl. Values of K_0^2 are calculated from the experimentally determined anisotropies for targets in which single-chance fission prevails, i.e., Bi^{209} and nuclides in the plutonium region. When values of K_0^2 for plutonium are compared with those from available neutron fission data, there is indicated an anomalous suppression of K_0^2 in the low-energy region below the values extrapolated from the higher energy data by plausible temperature dependences on excitation energy. Saddle-shape calculations and semiquantitative arguments which are reviewed lend added credence to the view that the saddle shape is independent of the mode of formation. The experimentally observed change in anisotropy with the fissionability parameter x is correlated with the effective moments of inertia at the saddle configuration (*vis-à-vis* scission point), indicating that thermodynamic equilibrium is first established near the saddle point in fission. Fission cross sections measured for Th^{232}, U^{233}, and U^{238} are supplemented by previously determined spallation cross sections to obtain total deuteron reaction cross sections. At 21 MeV the deuteron reaction cross section of heavy elements is found to be 1800 mb. The experimental reaction cross sections are compared with theoretical values calculated with a volume-absorption optical model.

I. INTRODUCTION

THEORETICAL formulations for the angular distribution of fission fragments from a single fissioning species have been derived, in the classical approximation, by various investigators beginning with Bohr[1] and Halpern and Strutinski.[2] Although the model neglects target and projectile spins, it approximates reasonably well the anisotropies obtained from a variety of experiments on fission induced by neutrons and by energetic charged particles (these and other developments in fission physics are discussed in various reviews).[3,4]

With excitation energies up to a few tens of MeV, fission spectra obtained in practice are usually derived from several species (distinguished by different excitation energies and A values) fissioning concurrently, due to the possibility of multichance neutron evaporation prior to fission. Following the development of Bohr,[1]

* Based on work performed under the auspices of the U. S. Atomic Energy Commission.

† Permanent address: Department of Physics, Wheaton College, Wheaton, Illinois.

‡ On leave from the Atomic Energy Establishment, Trombay, India, under sponsorship of the International Cooperation Administration.

[1] A. Bohr, in *Proceedings of the International Conference on the Peaceful Uses of Atomic Energy, Geneva, 1955* (United Nations, New York, 1956), Vol. 2, p. 151.

[2] I. Halpern and V. M. Strutinski, in *Proceedings of the Second International Conference on the Peaceful Uses of Atomic Energy, Geneva, 1958* (United Nations, Geneva, 1959), Vol. 15, p. 408.

[3] I. Halpern, Ann. Rev. Nucl. Sci. **9**, 245 (1959).

[4] J. R. Huizenga and R. Vandenbosch, *Nuclear Reactions* (North-Holland Publishing Company, Amsterdam, 1962), Vol. 2, Chapter 2, p. 42.

the angular distribution $W(\theta)$ of fission-fragment emission per unit solid angle for the composite spectrum from $n+1$ cofissioning species may be written as

$$W(\theta) \propto \sum_{i=0}^{n} \alpha_i \int_0^{I_m^{(i)}} dI \int_0^{I \sin\theta} dK\, f_i(K,I) \times[\sin^2\theta-(K^2/I^2)]^{-1/2}, \quad (1)$$

where θ is the direction of fission fragments relative to that of the beam direction. For the total vector angular momentum $\mathbf{I}=\mathbf{L}+\mathbf{I}_0+\mathbf{S}$, the projectile spin $\mathbf{I}_0$ and target spin $\mathbf{S}$ are neglected in Eq. (1) and $\mathbf{I}$ reduces to the angular momentum $\mathbf{L}$ originally brought in by the projectile diminished by the angular momentum carried off by neutron evaporation prior to fission. The projection of $\mathbf{I}$ on the nuclear symmetry axis is represented by $\mathbf{K}$. The function $f_i(K,I)$ gives the distribution in K and I of the particular species fissioning after emission of the ith neutron, $I_m^{(i)}$, being the maximum value of the angular momentum for this species. Each fractional coefficient α_i is obtained by dividing the number of fission events due to fission of the particular species resulting from emission of the ith neutron after formation of the compound nucleus by the total number of fission events arising from all $n+1$ species.

In order to evaluate $W(\theta)$ in Eq. (1), the angular distribution $W_i(\theta)$ for each species must be determined, as well as α_i. Numerical estimates involving assumed values of α_i for small n have led to successful reproduction of the experimentally observed $W(0°)/W(90°)$ anisotropy dependence on energy in the case of neutron-induced fission[5] and for fission induced by helium-ion bombardment.[6] The success of such numerical estimates depends much upon the presence of irregularities in the anisotropy dependence on excitation energy, which then serve as a guide for identifying the various ith-order thresholds as the anisotropy is expected to peak and drop off as a new threshold is reached. The coefficients α_i may be evaluated from level width ratios Γ_f/Γ_n (neglecting possible competition from photon emission), but these level width ratios are not uniquely determinable from the aforementioned numerical estimates, and generally are not known accurately enough from independent experimental methods[7] in the intermediate energy region where level widths for neutron emission and fission are comparable.

At present, the most reliable evaluations of Eq. (1) are obtainable when the conditions of fission are such that one of the coefficients α_i is so dominantly large that the others may be neglected. In practice, conditions for dominant α_0 are easiest to obtain with reasonable certainty. Large values of α_0 approaching unity are assured with highly fissionable species, i.e., large values of Z^2/A, and are also obtainable in regions of low fissionability where Γ_f/Γ_n is strongly dependent upon excitation energy.[8] The present work was undertaken to investigate the anisotropy of the fission fragment distribution from deuteron-induced fission for a few selected targets in the thorium-uranium region where α_0 is not necessarily dominant; and by including nuclides of very high fissionability and nuclides in the light element region where α_0 is dominantly large, it was desired to further probe various properties of the compound nucleus at the saddle point. In particular, it was of interest to compare saddle deformations in the light element region for fissioning nuclei produced by deuteron bombardment with comparable species obtained by helium-ion bombardment in previous work[9] at this laboratory.

The use of semiconductor detectors permits greater angular resolution and affords a generally increased sensitivity, in comparison to the conventional catcher-foil technique. Semiconductor detection was therefore utilized in this work so that, in addition to gross patterns, possible fine-structure effects could more easily be monitored. Further, while catcher foil techniques are generally limited to detection of certain fission products, semiconductor devices respond to the entire fission spectrum and permit the evaluation of fission cross sections, which may be compared with increasingly available reaction cross sections from optical-model calculations.

The optical model has been extensively used to interpret the elastic-scattering data[10,11] of projectiles such as protons, deuterons and alpha particles by various nuclei, with the objective of obtaining information on the strength and radial variation of the nuclear field. Most of such analyses have been done by two forms of the optical-model potential, viz., volume absorption[12] and surface-absorption[13,14] types. Although the optical model can usually be made to accommodate the elastic scattering, polarization, and reaction cross-section data, the parameters obtained from fits to only one type of data are not always unique and well understood.

One would like to test whether the information obtained on the strength and variation of the nuclear potential from elastic-scattering data gives reasonable results when applied to the study of other processes such as the stripping reactions and total-reaction cross sec-

[5] James J. Griffin, Phys. Rev. **116**, 107 (1959).
[6] R. Vandenbosch, H. Warhanek, and J. R. Huizenga, Phys. Rev. **124**, 846 (1961).
[7] R. Vandenbosch and J. R. Huizenga, in *Proceedings of the Second International Conference on the Peaceful Uses of Atomic Energy, 1958* (United Nations, Geneva, 1959), Vol. 15, p. 284.
[8] J. R. Huizenga, R. Chaudhry, and R. Vandenbosch, Phys. Rev. **126**, 210 (1962).
[9] R. Chaudhry, R. Vandenbosch, and J. R. Huizenga, Phys. Rev. **126**, 220 (1962).
[10] H. Feshbach, Ann. Rev. Nucl. Sci. **8**, 49 (1958).
[11] *Proceedings of the International Conference on the Nuclear Optical Model, Florida State University Studies No. 32*, edited by A. E. S. Green, C. E. Porter, and D. S. Saxon (The Florida State University, Tallahassee, Florida, 1959.)
[12] R. D. Woods and D. S. Saxon, Phys. Rev. **95**, 577 (1954).
[13] F. E. Bjorklund, S. Fernbach, and N. Sherman, Phys. Rev. **101**, 1832 (1956).
[14] F. Bjorklund and S. Fernbach, Phys. Rev. **109**, 1295 (1958).

tions. Optical-model analyses of the elastic-scattering data give an ambiguity in the determination of V, the real part of the central potential, and R, the nuclear radius, because only the product VR^2 is fixed. Since the reaction cross section is roughly proportional to R^2, a measurement of the reaction cross section can determine R alone and resolve the V-R ambiguity. Theoretical reaction cross sections calculated for alpha particles[15,16] with optical-model parameters deduced from elastic scattering have been found to agree quite well with the experimental total-reaction cross sections of heavy elements.[17] Several investigators[18–23] have measured 10-MeV proton reaction cross sections and compared their results with predictions of both volume and surface-absorption optical models where the parameters had been previously determined from analyses of elastic scattering. Although the total-reaction cross sections predicted by the surface-absorption model give slightly better agreement with the experimental results, it has not been established conclusively that other sets of Woods-Saxon parameters in the volume-absorption model might not fit the elastic scattering and total reaction cross-section data equally well. Recently Hinds *et al.*[24] have been reasonably successful in fitting deuteron and proton elastic-scattering data as well as deuteron-stripping data with a consistent set of optical-model parameters. Buck and Hodgson[25] have also made analysis of deuteron stripping with an optical model.

In this paper, we have measured the deuteron-fission cross sections and have estimated the total-reaction cross section by adding previous measurements of spallation cross sections. These experimental values of the deuteron-total reaction cross sections are compared with theoretical estimates based on the volume-absorption optical model using parameters[26,27] derived from analyses of elastic-scattering data.

II. EXPERIMENTAL PROCEDURES

Several fission experiments in the 7 to 11-MeV energy range were carried out in an 18-in. scattering chamber[28] with deuterons which were accelerated in the Argonne Tandem Van de Graaff. The bulk of the measurements, particularly those at higher energies up to 21 MeV, were made in an 11-in. scattering chamber with deuterons accelerated in the Argonne 60-in. cyclotron. In the cyclotron, deuterons of 21-MeV energy were degraded down to 8 MeV by means of a foil-degrading system, which also permitted determination of deuteron energies by range measurements. The characteristics of the collimating system employed were such that the image of the beam at the target was restricted to about $\frac{1}{8}$ in. Deuterons passing through the target were collected in a Faraday cup and the total charge was measured by a current integrator. With one gold surface-barrier detector positioned in the chamber at an angle corresponding to 90° from the beam direction in the center-of-mass system, the other detector was rotated independently in a horizontal plane for angular distribution measurements. Thin targets located at the center of the chamber were oriented with the normal to the target bisecting the angle between the two detectors, so that the fission fragments seen by each detector traversed equal thicknesses of target material.

Fission fragment pulses from charge-sensitive preamplifiers were fed through 150-ft cables to the main amplifiers, and then through single-channel analyzers operated in integral discrimination mode into a 256-channel analyzer for final sorting, display and recording. Single events were accumulated from each detector without coincidence requirements. Experimental details pertaining to beam characteristics, scattering chamber geometry, solid-state detector preparation and operation, target preparation and electronics systems, may be found in previous reports[6,8,9,17] by investigators at this laboratory.

III. EXPERIMENTAL RESULTS

The differential cross-section ratio was calculated at each angle relative to the 90° direction in the center-of-mass system by applying appropriate center-of-mass corrections to the count rates and angular positions. Assuming full momentum transfer of the projectile to the compound nucleus, center-of-mass corrections may be calculated from the dynamics of 2-fragment fission by applying the laws of conservation of momentum and of energy. Center-of-mass corrections are also available in tabulated form[29] for selected values of the relevant parameters. For each compound nucleus the average kinetic energy of the fragments in the center-of-mass system was calculated from the semiempirical expression[3] of Terrell, $\langle \mathrm{KE} \rangle = 0.121\ Z^2A^{-1/3}$ MeV. The center-

[15] George Igo, Phys. Rev. **15**, 1665 (1959).
[16] J. R. Huizenga and G. Igo, Nucl. Physics **29**, 462 (1962).
[17] J. R. Huizenga, R. Vandenbosch, and H. Warhanek, Phys. Rev. **124**, 1964 (1961).
[18] V. Meyer and N. M. Hintz, Phys. Rev. Letters **5**, 207 (1960).
[19] G. W. Greenslees and O. N. Jarvis, in *Proceedings of the International Conference on Nuclear Structure, Kingston, Canada, 1960*, edited by B. A. Bromley and E. Vogt (University of Toronto Press, Toronto, 1960), p. 217.
[20] R. D. Albert and L. F. Hansen, Phys. Rev. Letters **6**, 13 (1961); Phys. Rev. **123**, 1749 (1961).
[21] R. F. Carlson, R. M. Eisberg, R. H. Stokes, and R. H. Short, Bull. Am. Phys. Soc. **6**, 441 (1961).
[22] J. Wing and J. R. Huizenga, Phys. Rev. **128**, 280 (1962).
[23] B. Wilkins and G. Igo, Phys. Letters **3**, 48 (1962).
[24] S. Hinds, R. Middleton, and D. J. Pullen, Phys. Letters **1**, 12 (1962).
[25] B. Buck and P. E. Hodgson, Nucl. Physics **29**, 496 (1962).
[26] M. A. Melkanoff, in *Proceedings of the International Conference on the Nuclear Optical Model, Florida State University Studies No. 32*, edited by A. E. S. Green, C. E. Porter, and D. S. Saxon (The Florida State University, Tallahassee, Florida, 1959), p. 207.
[27] M. A. Melkanoff, T. Sawada, and N. Cindro, Phys. Letters **2**, 98 (1962).
[28] T. H. Braid and J. T. Heinrich (to be published).
[29] J. B. Marion, T. I. Arnette, and H. C. Owens, Oak Ridge National Laboratory Report, ORNL-2574, 1959 (unpublished).

of-mass corrections assumed equipartition of mass and energy between the fragments for average values.

The angular distribution of fission fragments from (d,xnf) reactions for the target nuclei Th^{232}, U^{238}, and U^{233} are, respectively, displayed in Figs. 1–3, via a plot of the differential cross-section ratio for full energy deuterons against center-of-mass angle. In the case of U^{238} and U^{233}, the differential cross-section ratio is also plotted for 13-MeV deuterons. All data for the anisotropies in Figs. 1–3 were obtained with the 11-in. scattering chamber by cyclotron-accelerated deuterons. The anisotropy $W(174°)/W(90°)$ as a function of deuteron energy in laboratory coordinates is shown in Figs. 4–6 for the respective targets Th^{232}, U^{238}, and U^{233}. In the case of U^{238} and U^{233}, additional data in the 7- to 11-MeV region were obtained with deuterons accelerated by the tandem Van de Graaff accelerator, and are plotted as separate points. The error shown for each of the experimental points in Figs. 1–6 represents the standard deviation of counting statistics. This error assumes larger values for low energies in Figs. 4–6 because of reduction in deuteron beam intensity, which could not be compensated for by increased bombardment times.

For each of the angular distributions shown in Figs. 1–3, an analytical fit has been made with the simple anisotropy expression $W(\theta)/W(90°)=1+(b/a)\cos^2\theta$, equivalent to an even-term Legendre polynomial expansion up to $P_2(\cos\theta)$. This simple expression reproduces the experimental data plotted in Figs. 1–3 reasonably well at all angles. On this basis of the demonstrated validity of the expression $W(\theta)/W(90°)=1+(b/a)\cos^2\theta$ as a good approximation to the angular distribu-

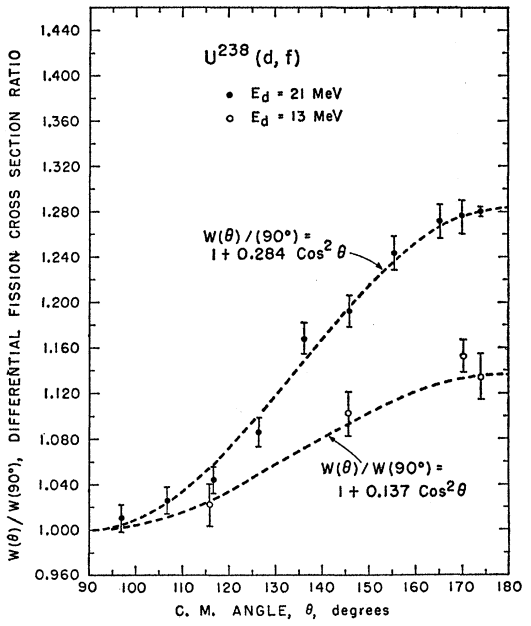

FIG. 2. Ratio of the differential fission cross section, $W(\theta)/W(90°)$, as a function of the center-of-mass angle in degrees, for deuteron-induced-fission of U^{238} at deuteron energies of 13 and 21 MeV. The plotted points are experimental values with statistical uncertainties. The dashed curve at each energy is an analytical fit for the expression $W(\theta)/W(90°)=1+C\cos^2\theta$.

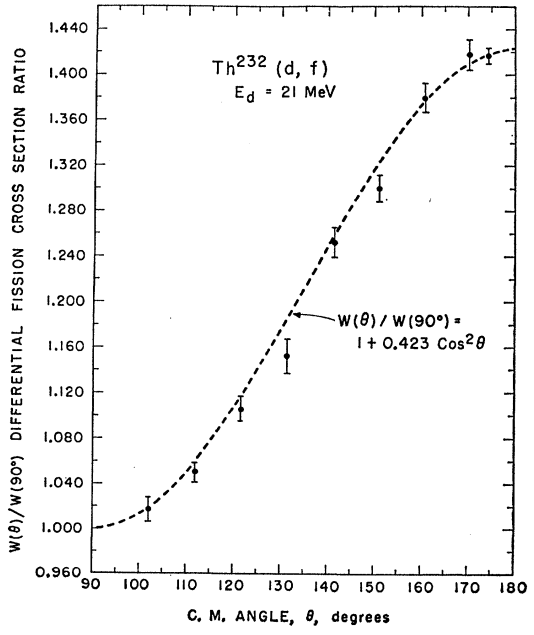

FIG. 1. Ratio of the differential fission cross section, $W(\theta)/W(90°)$, as a function of the center-of-mass angle in degrees for deuteron-induced fission of Th^{232} at 21 MeV. The plotted points are experimental values with statistical uncertainties. The dashed curve is an analytical fit for the expression $W(\theta)/W(90°)=1+0.423\cos^2\theta$.

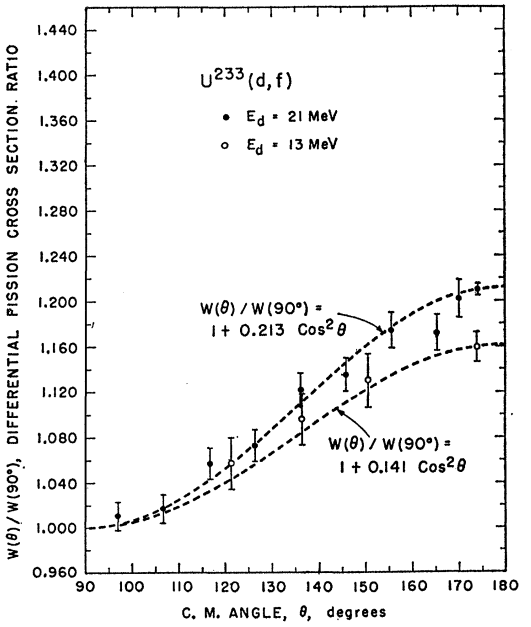

FIG. 3. Ratio of the differential fission cross section, $W(\theta)/W(90°)$, as a function of the center-of-mass angle in degrees for deuteron-induced fission of U^{233} at deuteron energies of 13 and 21 MeV. The plotted points are experimental values with statistical uncertainties. The dashed curve at each energy is an analytical fit for the expression $W(\theta)/W(90°)=1+C\cos^2\theta$.

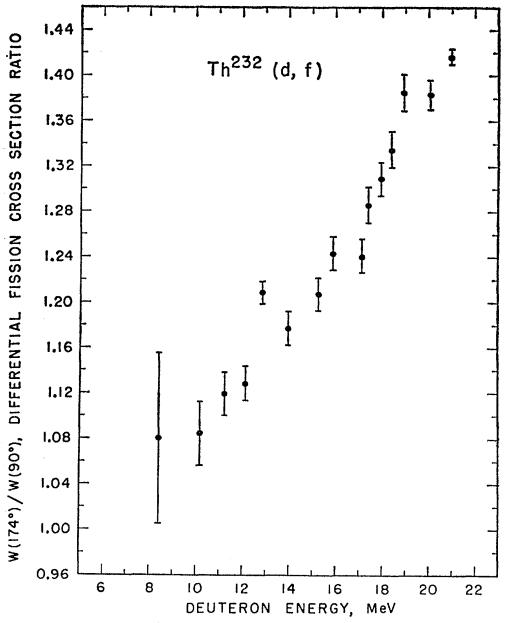

FIG. 4. Differential fission cross section ratio, $W(174°)/W(90°)$, for deuteron-induced fission of Th^{232} as a function of deuteron energy in the laboratory system.

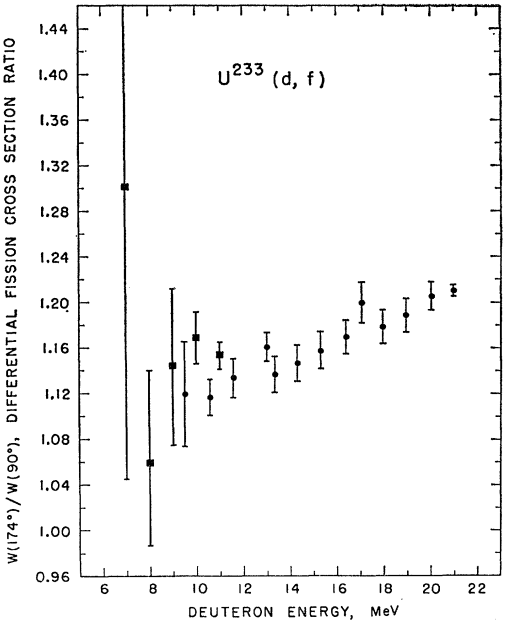

FIG. 6. Differential fission cross-section ratio, $W(174°)/W(90°)$, for deuteron-induced fission of U^{233}, as a function of deuteron energy in the laboratory system. Five low-energy points (squares) obtained with deuterons accelerated in tandem Van de Graaff, remainder by cyclotron (solid circles).

tion, the differential cross sections may be integrated over θ to obtain the fission cross section, σ_f. Excitation functions for σ_f thus determined are displayed for the target nuclei Th^{232}, U^{238}, and U^{233} in Figs. 7–9. The deuteron energy used for the abscissa in Figs. 7–9 is expressed in laboratory coordinates. The statistical error is shown for the cross sections only when the error exceeds the geometric size of the plotted point. Numerical values of the anisotropies and cross sections at cyclotron

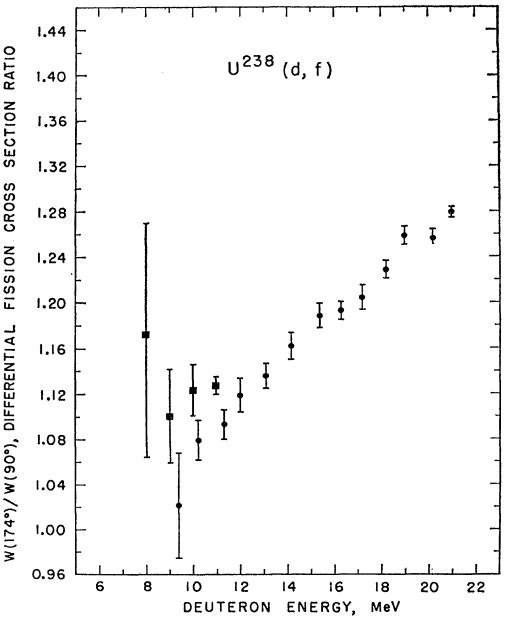

FIG. 5. Differential fission cross section ratio, $W(174°)/W(90°)$, for deuteron-induced fission of U^{238}, as a function of deuteron energy in the laboratory system. Four low-energy points (squares) obtained with deuterons accelerated in tandem Van de Graaff, remainder by cyclotron (solid circles).

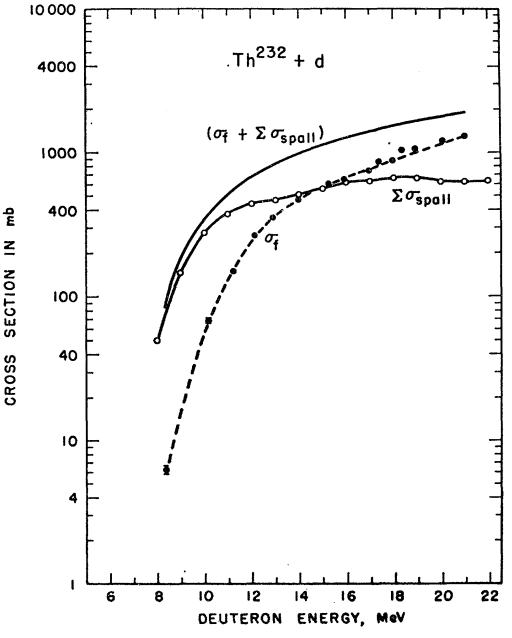

FIG. 7. Th^{232} excitation functions for deuteron-induced fission (this work) and spallation (calculated and compiled from the literature, see text).

TABLE I. Cross sections and anisotropy values for 21-MeV deuteron-induced fission.

Target nucleus	$W(174°)/W(90°)$ center of mass	σ_f (mb)
Plutonium-239	1.202±0.018[a]	...
Neptunium-237	1.184±0.018	...
Uranium-233	1.210±0.015	1580±5[b]
Uranium-234	1.229±0.019	...
Uranium-235	1.192±0.018	...
Uranium-236	1.240±0.019	...
Uranium-238	1.280±0.018	1330±5
Thorium-232	1.417±0.022	1300±7
Bismuth-209	1.446±0.022	0.036±0.001
Lead-206 (enriched)	1.515±0.082	0.0050±0.0004
Thallium (natural)	1.585±0.276	0.0025±0.0004

[a] Errors cited for anisotropies include random in addition to statistical errors.
[b] Cross section errors include statistics only.

TABLE II. Fission anisotropies for 11-MeV Van de Graaff deuterons.

Target nucleus	$W(172°)/W(90°)$ center of mass
Plutonium-239	1.122±0.012[a]
Neptunium-237	1.110±0.011
Uranium-233	1.152±0.012
Uranium-234	1.181±0.011
Uranium-235	1.139±0.011
Uranium-236	1.146±0.014
Uranium-238	1.127±0.008
Thorium-232	1.194±0.018

[a] Statistical error only.

full energy for all the target nuclides studied are tabulated in Table I. Table II shows anisotropies for various heavy element targets obtained with tandem Van de Graaff 11-MeV deuterons.

Self-absorption of fission fragments in the various thin targets employed in this work has previously been shown to be negligible.[8] The cross sections in Figs. 7–9 are plotted for an assumed monoenergetic deuteron beam, taking each energy to be that of the mean value of the energy distribution. Energy dispersion of deuterons accelerated in the tandem Van de Graaff generator is negligible for purposes of this work. Measurements of deuteron beam dispersion at the Argonne cyclotron[30] show a full width at half-maximum intensity of less than 0.2 MeV at 21 MeV, and a corresponding dispersion approaching 0.7 MeV for 8-MeV deuterons. While the assumption of a monoenergetic beam may introduce relatively small errors over most of the energy range for cyclotron-accelerated deuterons, at low energies the plotted cross sections may exceed the true value for a nonvanishing beam width by amounts roughly comparable to the statistical error.

[30] W. J. Ramler, J. L. Yntema, and M. Oselka, Nucl. Instr. Methods 8, 217 (1960).

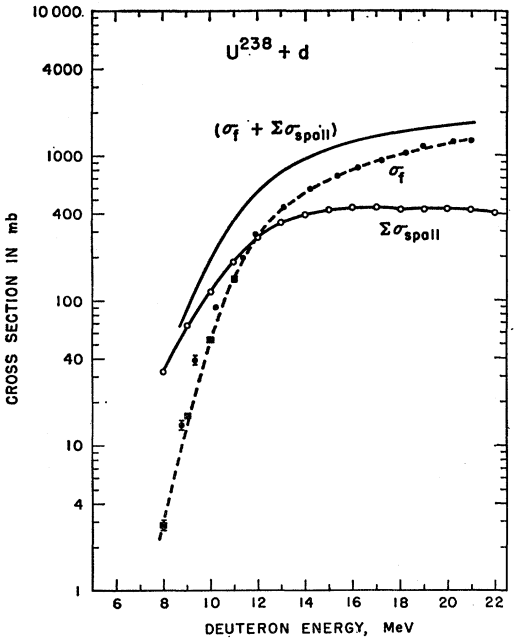

FIG. 8. U^{238} excitation functions for deuteron-induced fission (this work) and spallation (calculated and compiled from the literature, see text). ● Cyclotron; ■ tandem Van de Graaff.

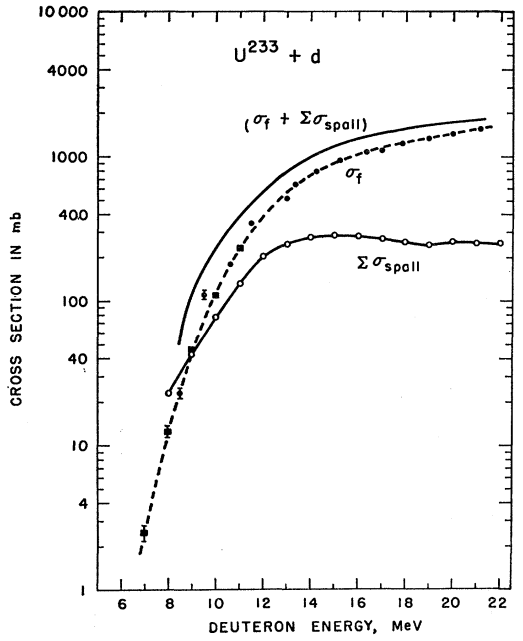

FIG. 9. U^{233} excitation functions for deuteron-induced fission (this work) and spallation (calculated and compiled from the literature, see text). ● Cyclotron; ■ tandem Van de Graaff.

IV. DISCUSSION

A. Anisotropies

Comparison of the anisotropies in Table I with the corresponding values of Coffin and Halpern[31] obtained

[31] C. T. Coffin and I. Halpern, Phys. Rev. 112, 536 (1958).

by the catcher-foil technique shows good agreement. However, the energy dependence of the anisotropy shown for $Th^{232}(d,xnf)$ in Fig. 4 is much more pronounced than that obtained by Coffin and Halpern for the same reaction. The reasons for this disparity are not evident. The small rise in the Th^{232} anisotropy at 13 MeV was observed in two different sets of data on different dates, but the possibility of a purely statistical fluctuation cannot be ruled out until further data in this energy region are obtained.

The anisotropies shown in Table II for fission induced by 11-MeV deuterons are generally reduced in value from those obtained at 21 MeV. The considerable reduction in angular momentum explains the more isotropic distribution obtained at 11 MeV. Moreover, the systematic trend observable from species to species at 21 MeV is no longer evident among the anisotropies at 11 MeV. The relatively small differences in anisotropy obtained at 11 MeV do not support a discriminating interpretation at this time.

By adjusting the parameters in Eq. (1) to match the calculated anisotropy with the experimental curves, the data of Figs. 4–6 are potentially useful for determination of nuclear characteristics related to fission. For example, if the values of α_i were correctly ascertained, it would, in principle, be possible to evaluate K_0^2, the average square of the Gaussian K distribution, as a function of excitation energy. However, the values of α_i are not uniquely determinable from these data alone and an unambiguous evaluation of K_0^2 must await further resolution of these parameters.

1. Dependence on Fissionability Parameter and Energy

The Th^{232} anisotropy versus energy curve in Fig. 4 may be compared with the corresponding curves for U^{238} and U^{233} shown in Figs. 5 and 6, respectively. In order of increasing fissionability parameter, Z^2/A, the anisotropy of these nuclides falls in the ascending order Th^{232}, U^{238}, and U^{233}. It is seen that the energy dependence of the anisotropy increases in the opposite direction, from a mild dependence for U^{233} in Fig. 6 to the strongest energy dependence for Th^{232} in Fig. 4. The anisotropy energy curve shown here for U^{233} is similar to that for Np^{237} given by Coffin and Halpern,[31] as may be expected from the fact that the value of the fissionability parameter, Z^2/A, for Np^{237} is very close to that of U^{233}.

The $W(\theta)/W(90°)$ dependence on θ is shown in Figs. 1–3. The most pronounced variation in angular distribution is shown for Th^{232}, with U^{233} displaying the least variation and U^{238} occupying an intermediate position. Following presently accepted theory, the variation in anisotropy between the three nuclides may be qualitatively explained in terms of differences in temperature and of the variation of effective moments of inertia of the fissioning nuclei. Given the excitation energy as determined from projectile energy, Q balance and the fission barrier, both dependences follow from statistical analysis predicated on the Fermi gas model. Such analysis leads to the derivation of the relation $K_0^2=T\mathcal{I}_{\text{eff}}/\hbar^2$, where T is the thermodynamic temperature and $\mathcal{I}_{\text{eff}}$ is the effective moment of inertia of the fissioning nucleus at the saddle point. According to the Fermi gas model, $T\propto E^{1/2}$, for large values of E, where E is the excitation energy. The effective moment of inertia $\mathcal{I}_{\text{eff}}$ is defined as $\mathcal{I}_\perp\mathcal{I}_{\parallel}/(\mathcal{I}_\perp-\mathcal{I}_{\parallel})$, where $\mathcal{I}_\perp$ and $\mathcal{I}_{\parallel}$ are the perpendicular and parallel moments of inertia, respectively. When the anisotropy is evaluated in terms of the angular distribution function of Halpern and Strutinski,[2] it can be shown to increase as K_0^2 decreases (see Fig. 12). From the definition of K_0^2, it further follows that if the temperature varies as the square root of the excitation energy, the anisotropy decreases with increasing excitation energy.

Thus in the case of U^{233}, which is the most fissionable of the three species, the prevailing early chance fissions (hence, high-excitation energies with correspondingly large values of K_0^2) account in part for the reduced anisotropy observed. Thorium on the other hand is the least fissionable of the three and with a greater percentage of later chance fission, the reduced K_0^2 values contribute to the larger anisotropy observed.

The second factor contributing to the observed variation of anisotropy among the targets Th^{232}, U^{238} and U^{233} is to be found in the dependence of K_0^2 on the effective moment of inertia, $\mathcal{I}_{\text{eff}}$. Liquid-drop model calculations by Cohen and Swiatecki[32] and Strutinski *et al.*[33] indicate that in the region of heavy elements the saddle deformation increases (corresponding to decreasing $\mathcal{I}_{\text{eff}}$) with decreasing fissionability (see Fig. 13). Thus, in considering the compound nuclei corresponding to target nuclei U^{233}, U^{238}, and Th^{232}, the Cohen and Swiatecki model predicts decreasing values of the effective moments of inertia in the order named. The consequent reduction in value of K_0^2 therefore also contributes to the increasing anisotropy of the series U^{233}, U^{238}, and Th^{232}. The energy dependence of the anisotropy in Figs. 4–6 may be qualitatively interpreted in terms of the opposing effects of decreasing angular momentum brought in by deuterons of decreasing energy, and of decreased excitation energy. The angular momentum effect prevails and in each case the anisotropy diminishes with decreasing deuteron energy. The very weak energy dependence of the U^{233} anisotropy is noteworthy, especially in the energy region below 10 MeV where the U^{233} anisotropy values compare favorably with, and possibly exceed, those of Th^{232} and U^{238}.

In considering the explicit dependence of K_0^2 on excitation energy, some limiting arguments bearing on the K_0^2 energy dependence may be advanced from selected

---

[32] S. Cohen and W. J. Swiatecki, Ann. Phys. (N. Y.) **19**, 67 (1962); also, private communication.

[33] V. M. Strutinski, N. Ya. Lyashchenko, and N. A. Popov (private communication).

data. The dependence of K_0^2 on excitation energy in the plutonium region is shown in Fig. 10. Since the compound nuclei involved have the same Z and similar A values, the fissionability parameter Z^2/A is essentially constant, and the nuclides compared, therefore, provide a true measure of the dependence of K_0^2 on excitation energy. Values of K_0^2 in the low-energy region are from the Los Alamos $Pu^{239}(n,f)$ data,[34] while the two high-energy points were calculated from deuteron and helium ion anisotropy data obtained at this laboratory. The latter two points have been plotted at the initial excitation energy and cannot be considered to be exact because of the uncertainty in the number of neutrons evaporated prior to fission. However, by assuming 100% first chance fission, which is a good first approximation in this mass region of high fissionability, the points obtained are valid lower limits of K_0^2 since contributions from higher order fission would tend to elevate values of K_0^2 for the particular excitation energies which are plotted in Fig. 10. Also shown in Fig. 10 are three theoretical curves based on varying assumptions of dependence of temperature on energy, as indicated in the figure. Each of the three curves is normalized to the highest energy point. Qualitative consideration of the information in the figure leads to the conclusion that none of the three temperature relations can be harmonized with both the high- and low-energy points without allowing for a reduction in the effective moment of inertia in the low-energy region. In contrast to this result, it should be observed that the $Bi^{209}(\alpha,f)$ data of Chaudhry *et al.*[9] do not indicate a suppression of K_0^2 for excitation energies as low as 5 MeV. The latter nucleus has a smaller fissionability parameter x and is in a region where the saddle and scission configurations are similar.

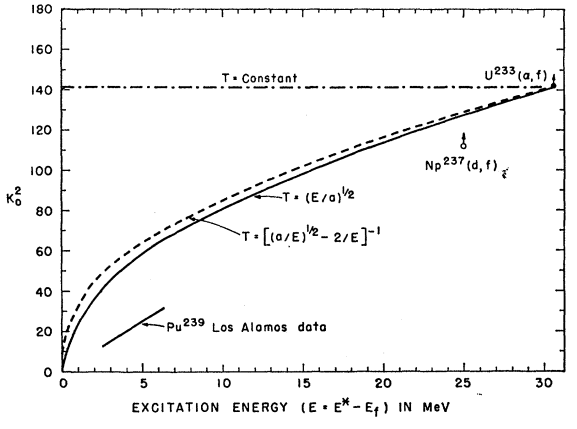

FIG. 10. Variation of K_0^2 with excitation energy for various compound nuclei of plutonium, based on three assumed relations of temperature dependence on energy as shown, normalized to the point U^{233} (α,f). Values of $I_m^2=2\langle I^2\rangle=134$ for $Np^{237}(d,f)$ [this work] and $I_m^2=2\langle I^2\rangle=425$ for $U^{233}(\alpha,f)$ [Chaudhry *et al.*, Ref. 9] used to calculated K_0^2 were obtained by optical-model calculations. $Pu^{239}(n,f)$ data are from the work of several groups at Los Alamos.[34]

[34] L. Blumberg and R. B. Leachman, Phys. Rev. **116**, 102 (1959); also, private communication from J. E. Simmons and J. J. Griffin.

2. *Radium Anomaly*

A conventional plot of the observed anisotropies at full cyclotron energy of 21 MeV as a function of Z^2/A for the compound nucleus is shown in Fig. 11 for all the target nuclei studied in this work. The distribution of points in the transradium region is similar to that obtained by Coffin and Halpern[31] and displays for the subradium elements a rise in anisotropy equaling or exceeding that of Th^{232}. There is little or no direct empirical evidence to account for suppression of anisotropy in the radium region. In order to develop the implications of this suppression, the assumptions which form the basis of the viewpoint here adopted are first reviewed: (1) Although K is not a good quantum number for the transition from the compound nucleus to the saddle point, the distribution in K is assumed to be frozen in at the saddle point and conserved through the scission point. (2) The anisotropy of a given fissioning species is determined completely by K_0^2 and $F(I)$, where $F(I)$ is the spin distribution. (3) K_0^2 is in turn uniquely determined by the effective moment of inertia at the saddle point and by the temperature according to the relation $K_0^2=\mathcal{I}_{\text{eff}}T/\hbar^2$. (4) The saddle deformation, characterized by $\mathcal{I}_{\text{eff}}$, is a property of each nuclear species independent of mode of formation. (5) Where the possibility of neutron evaporation before fission exists, the fissionability of each species in the chain, as determined by the level width ratio Γ_f/Γ_n, will also affect the net angular distribution. Γ_f/Γ_n in turn depends on the relative heights of the fission barrier

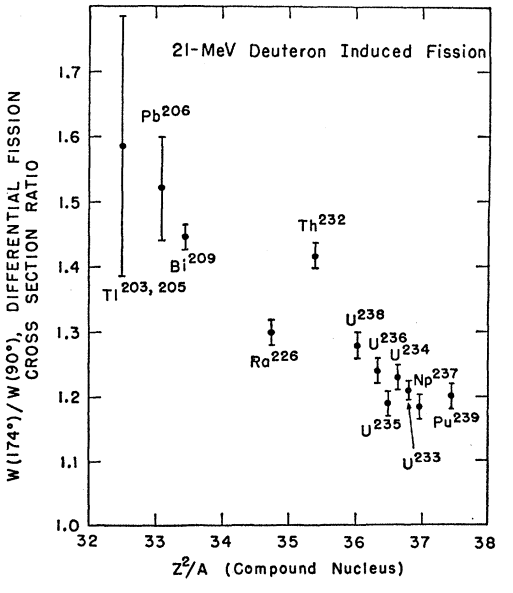

FIG. 11. Variation of fission-fragment anisotropies for deuteron-induced-fission in various target nuclides (as labeled) as a function of Z^2/A for the compound nucleus.

and the neutron binding energy, slowly changing or constant with energy in the heavy element region and rising sharply with energy in the light element region. If the K distribution is not established at the saddle deformation but at some other deformation (e.g., the scission deformation), a similar group of assumptions follows for this critical deformation. Some discussion of the interpretation of the experimental anisotropies as a function of the relative fissionability parameter x in terms of whether the K distribution is established at saddle or scission deformation will be given later.

According to the assumptions enumerated, the decrease in anisotropy at Ra^{226} is interpreted as being associated with an increase in the temperature (i.e., the fission spectrum is dominated by α_0 and α_1 events of high excitation energy). This interpretation further assumes that in the Ra^{226} region the effective moment of inertia does not depart from the regular variation predicted by the models of Cohen and Swiatecki and of Strutinski (this effect alone predicts the anisotropy for Ra^{226} to be larger than for Th^{232}), and that no large changes in $\langle I^2\rangle$ occur for the region from Pb to U, together with negligible target spin-dependence effects for these species. The further rise in anisotropy as the light element region is approached in Fig. 11 is attributed to continued reduction in the effective moment of inertia and in the temperature. The latter effect arises primarily from the marked increase in the fission threshold for elements in the Bi region.

Radium fission spectra observed in our work were dominantly symmetric with a small contribution of asymmetric fission clearly in evidence. The origin and cause of fission mode are not yet well defined and mode of fission is here regarded as a secondary rather than a primary property for anisotropy. It is postulated that the nature of the mass split is determined between the saddle and scission points, possibly very close to the latter. According to present experimental evidence [35–38] no direct relation independent of temperature (or excitation energy) has been shown to exist between anisotropy of the fission fragment distribution and asymmetry of the mass split.

B. Saddle Deformation and Modes of Formation in the Light Element Region

If consideration is now given to the light element region, it is of particular interest to compare the saddle-point deformations for fissioning nuclei produced by deuteron capture with those obtained by helium ion bombardment[9] of targets in this mass region. The light element region lends itself to such analysis because fission processes here have been established as predominantly, if not exclusively, first chance events.

The saddle deformation may be conveniently displayed in terms of the ratio $\mathcal{I}_{\rm sph}/\mathcal{I}_{\rm eff}$, where $\mathcal{I}_{\rm eff}$ is the effective moment of inertia (defined previously) at the saddle point, and $\mathcal{I}_{\rm sph}$ is the moment of inertia of a sphere of equal volume. $\mathcal{I}_{\rm eff}$ may be calculated from K_0^2 for a known temperature as previously indicated. K_0^2 in turn may be evaluated from the experimentally determined anisotropy by a relationship deduced from the Halpern-Strutinski angular distribution function[2]

$$W_{I,K0}=(2/\pi)^{1/2}(N/2\pi)(I/2K_0)[\exp(-I^2\sin^2\theta/4K_0^2)]\times J_0(iI^2\sin^2\theta/4K_0^2). \quad (2)$$

The availability of transmission coefficients for various projectile-nucleus potential systems makes possible an evaluation of the anisotropy by means of Eq. (2) with exact weighting coefficients for the various angular momentum terms; thus,

$$W(180°)/W(90°)=\left[\sum_{l=0}^{l_{\rm m}} l(2l+1)T_l\right]\times\left\{\sum_{l=0}^{l_{\rm m}}[l(2l+1)T_l]\exp\left(-\frac{\beta I^2}{2}\right)J_0\left(\frac{i\beta I^2}{2}\right)\right\}^{-1}. \quad (3)$$

If the projectile and target spins are neglected compared to the orbital angular momentum l, then in Eq. (3) the angular momentum, I, of the nucleus at the saddle point is equal to l, and is therefore treated as a summation parameter. In Eq. (3), T_l are the transmission coefficients, and J_0 is the zero-order Bessel function with an imaginary argument indicated by the factor $i\equiv(-1)^{1/2}$. In this equation, $\beta\equiv 1/2K_0^2$. Since the number of nonvanishing angular momentum terms is limited, Eq. (3) may be conveniently evaluated by carrying out the indicated summations with the aid of tabulated values of the exponential and Bessel functions. Inasmuch as Eq. (3) neglects projectile and target spins, the anisotropies calculated therefrom are modified by a spin-correction factor due to Griffin[39]:

$$\{1+(\beta^2/18)I_m(I_m+2)[I_0(I_0+1)+S(S+1)]\}^{-1}, \quad (4)$$

where I_0 and S are the target and projectile spins, respectively, I_m is the maximum projectile angular momentum, and $\beta=1/2K_0^2$.

The spin-corrected anisotropies are calculated for a range of assumed values of K_0^2 and plotted in Fig. 12 for the $Bi^{209}(d,f)$ reaction. In this case, $I_0=9/2$ and $S=1$. The magnitude of the spin correction was generally less than 5% of the anisotropy. The variation of the anisotropy with K_0^2 is dependent upon the model assumed for the d-Bi^{209} potential function, as indicated by the four curves plotted in Fig. 12. Three of the curves

[35] K. F. Flynn, L. E. Glendenin, and J. R. Huizenga, Bull. Am. Phys. Soc. **7**, 303 (1962).
[36] J. H. Manley, Nucl. Phys. **33**, 70 (1962).
[37] B. D. Kuz'minov, L. S. Kutsaeva, and I. I. Bondarenko, Zh. Eksperim. i Teor. Fiz. **42**, 105 (1962) [translation: Soviet Phys.—JETP **15**, 75 (1962)].
[38] I. A. Baranov, A. N. Protopopov and V. P. Eismont, Zh. Eksperim. i Teor. Fiz. **41**, 1003 (1961) [translation: Soviet Phys.—JETP **14**, 713 (1962)].
[39] James J. Griffin, Phys. Rev. **127**, 1248 (1962).

are based on transmission coefficients calculated with optical-model parameters, while the fourth derives from the square-well model. The relevant parameters for each case are shown in the figure, along with the cross section and mean square angular momentum required by the given parameters. One set of optical-model parameters[26] is from analysis of 15-MeV deuteron elastic scattering on lead ($V=-48.5$ MeV, $W=-9$ MeV, $a=0.63$ F and $r_0=1.52$ F) and another set[27] is from similar analyses of 21-MeV deuterons on gold ($V=-60$ MeV, $W=-18$ MeV, $a=0.59$ F and $r_0=1.50$ F). The third set is obtained from the first set by arbitrarily reducing r_0 but keeping Vr_0^2 fixed. As seen in the figure, the uncertainty reflected in K_0^2 for the above range in parameters at the experimentally determined anisotropy of $Bi^{209}(d,f)$ is of the order of 20%.

Values of the saddle deformation calculated with the two extreme values of K_0^2 from the optical-model calculations are shown in Fig. 13, as a function of the relative fissionability parameter, $x=(Z^2/A)/(Z^2/A)_0$. Also shown are plots of saddle deformations for several compound nuclei obtained in this region by helium ion bombardment in the work of Chaudhry *et al.*[9] A theoretical curve for saddle deformations deduced by Cohen and Swiatecki[32] and Strutinski *et al.*[33] from liquid-drop model calculations is also shown to permit comparison with the experimental data.

Within the limits of uncertainty of the optical-model parameters, it is seen from Fig. 13 that the saddle deformation corresponding to $Bi^{209}(d,f)$ definitely falls in the trend of deformations produced by helium ion bombardment. This is taken as further supporting evidence of the assumption that the saddle-point characteristics are intrinsic to the species involved, independent of the mode of formation of the saddle deformation.

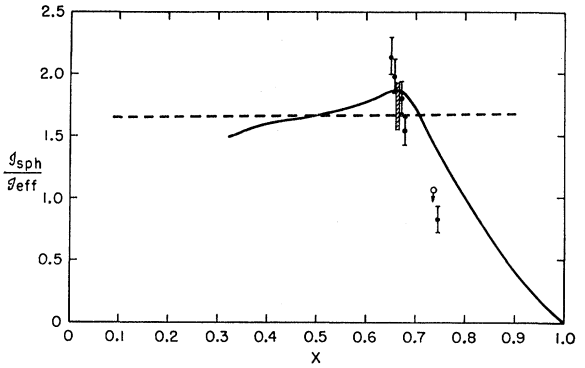

FIG. 13. Comparison of saddle deformations produced by deuteron excitation (shaded rectangle and open circle) and by helium ion excitation (closed circle) as a function of the relative fissionability parameter $x=(Z^2/A)/(Z^2/A)_{crit}$. One deuteron point represents extreme values obtained from several sets of transmission coefficients (Fig. 12) using the $Bi^{209}(d,f)$ anisotropy determined in this work. The other deuteron point (open circle) is from the $Np(d,f)$ anisotropy data and the assumption of 100% 1st chance fission (hence the upper limit in $\mathcal{I}_{sph}/\mathcal{I}_{eff}$). The helium ion points are from data of Chaudhry *et al.* (Ref. 9). Temperatures at the saddle configurations were computed with the Fermi gas level density parameter $a=A/8$. Theoretical predictions of the critical deformation at the saddle point (——) and at the scission point (– – –) are based on the charged liquid-drop model calculations by Cohen and Swiatecki (Ref. 32), and by Strutinski (Ref. 33).

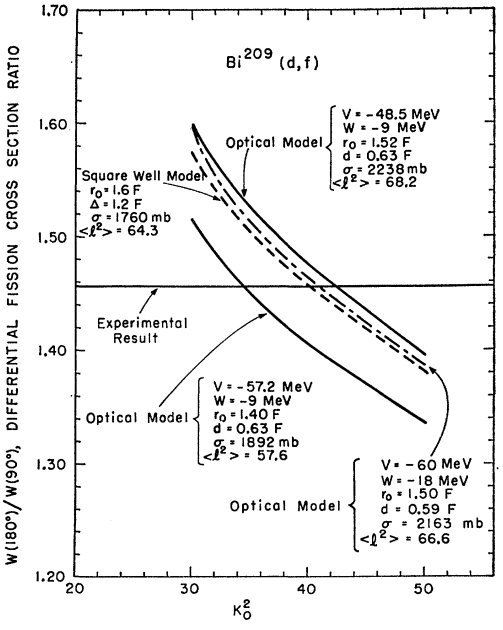

FIG. 12. Variation of theoretical anisotropy, $W(180°)/W(90°)$, with K_0^2, based on several sets of deuteron transmission coefficients for a Bi^{209} target as determined by a square-well model and by optical-model calculations, parameters as indicated. The horizontal line represents the experimental anisotropy.

C. Relation of Anisotropy to Saddle and Scission Configurations

With the fissioning nucleus in a given state of angular momentum, the relation $K_0^2=\mathcal{I}_{eff}T/\hbar^2$ indicates that for a constant temperature, the anisotropy is determined by the degree of nuclear deformation reflected through $\mathcal{I}_{eff}$. Strutinski[33] has recently reviewed the question as to which particular deformation of the fissioning nucleus determines the angular distribution of the fission fragments, i.e., whether, for example, the saddle deformation fixes the angular distribution, or whether a deformation closer to the scission point is the critical factor in determining anisotropy.

The solid curve in Fig. 13 shows the variation in $\mathcal{I}_{sph}/\mathcal{I}_{eff}$ (where $\mathcal{I}_{sph}$ is the moment of inertia of a spherical nucleus of equal volume) calculated by Cohen and Swiatecki[32] and Strutinski[33] from saddle-point deformations for different values of the relative fissionability parameter x. The dashed curve in the figure illustrates the variation in $\mathcal{I}_{sph}/\mathcal{I}_{eff}$ with x for the scission-point deformations calculated by Strutinski.[33]

If the fission fragment angular distribution is fixed at the scission point, one must assume equilibrium in K_0^2

as well as thermal equilibrium as the scission point is approached. Nonaxially symmetric deformations and Coriolis forces might serve to mix the K distribution beyond the saddle point.

The plotted points in Fig. 13 represent values of the ordinate calculated from experimentally measured anisotropies for deuterons in this work and for alpha particles in previous work[9] at this laboratory. The saddle-point temperatures used in converting the K_0^2 values to the corresponding ϑ_{eff} values were derived with a Fermi gas level density parameter $a=A/8$. It is seen that while the effective moments calculated for scission-point deformations show a flat dependence on x for all values of x, the experimentally determined values exhibit a strong dependence on x for large x, which closely parallel that of the values calculated from saddle-point deformations. In a more accurate comparison of the experimental data with the dashed curve, the scission-point temperatures should be used in converting our experimental values of K_0^2 to the values of ϑ_{eff}. This correction raises the values of $\vartheta_{\text{sph}}/\vartheta_{\text{eff}}$ for the points at larger x values but not nearly enough to alter the above argument. In the approximate range $x\leq 0.7$ it is seen from Fig. 13 that the effective moments predicted by both models are comparable; this observation is consistent with the finding[40] that in the light element region the calculated saddle- and scission-point configurations closely agree. It is concluded that insofar as the assumptions inherent in the calculated moments permit a valid comparison with the experimental data, these data support the view that when an appreciable difference in the saddle- and scission-point configuration exists, the angular distribution of fission fragments is determined by the effective moment of inertia at the saddle point.

These conclusions are based on the use of rigid-body moments of inertia. Attempts have been made to estimate the effects of shell structure on the predicted moments using the effective neutron and proton densities of Newton.[41] The assumption is made that the shell structure persists into the deformed and excited saddle and scission configurations. For the case where the anisotropy is assumed to be determined at the scission configuration, the addition of shell structure leads to the prediction that the fission fragments from plutonium will have a greater anisotropy than those from elements in the region of lead for the same $\langle I^2\rangle$ and temperature. This postulate is therefore in disagreement with the experimental results.

The conclusion that the K_0^2 values are determined by the saddle configuration is consistent with a fast nonequilibrium process beyond the saddle point but does not require it. The possibility exists that thermal equilibrium is maintained from saddle to scission but that K_0^2 is constant beyond the saddle due to the lack of forces which cause K mixing. It should also be emphasized that the effective moments of inertia plotted in Fig. 13 were determined at rather large excitation energies. The reduced values of K_0^2 for plutonium at low excitation energies might be interpreted as partially due to the freezing in of K_0^2 nearer the scission shape, although the pairing correlation seems to be the more acceptable explanation of the anomaly at this time. Nuclei with x less than 0.7 are completely insensitive to whether the K_0^2 distribution is established at the saddle or scission configurations, and hence, on this basis would not be expected to show a K_0^2 anomaly at low excitation energies, although arguments can also be made to show that the pairing correlations for these nuclei would be greatly reduced. Thus, the experimental results of the energy dependence of K_0^2 are consistent with either a pairing effect or the establishment of the K_0^2 distribution nearer the scission configuration for low energies.

D. Cross Sections

The relative contributions of deuteron-induced fission and spallation to the total reaction cross sections for Th^{232}, U^{238}, and U^{233} are shown in Figs. 7, 8, and 9, respectively. It may be noted that the experimental fission cross sections for U^{233} and U^{238} in the low-energy region obtained with Van de Graaff-accelerated deuterons are slightly displaced from those obtained with cyclotron-accelerated deuterons. The reason for this displacement may be due to both a small uncertainty in the cyclotron beam energy and a distortion of the average cross section arising from severe dispersion of the cyclotron beam degraded to low energies. In any event, the Van de Graaff data are probably most nearly correct because of better sharpness and control of beam energy.

Since a substantial body of experimental data is available on the deuteron-induced spallation cross sections for the heavy elements Th^{232}, U^{238}, and U^{233} over a large energy range, deuteron cross sections of these three species were compared with reaction cross sections computed with a volume-absorption optical model. With these nuclides most of the total reaction cross section is due to the processes (d,f), (d,n), $(d,2n)$, $(d,3n)$, $(d,4n)$, $(d,\alpha n)$, (d,p), and (d,t). Of these, the (d,f) process forms the major part of the reaction cross section. In the case of Th^{232} the spallation cross sections $\sigma(d,p)$ and $\sigma(d,n)$ have been measured by Slater.[42] For U^{238}, $\sigma(d,p)$ has been measured by Wing *et al.*[43] and also by Slater[42]; $\sigma(d,2n)$, $\sigma(d,4n)$, and $\sigma(d,t)$ have been measured by Wing *et al.*[43] The cross sections $\sigma(d,n)$, $\sigma(d,2n)$, $\sigma(d,3n)$, and $\sigma(d,\alpha n)$ have been measured for U^{233} by Gibson[44] and also by Foreman *et al.*[45]

[40] R. Vandenbosch and J. R. Huizenga, Phys. Rev. **127**, 212 (1962).

[42] L. M. Slater, University of California Radiation Laboratory Report UCRL-2441, 1954 (unpublished).

[43] J. Wing, W. J. Ramler, A. L. Harkness, and J. R. Huizenga, Phys. Rev. **114**, 163 (1959).

[44] W. M. Gibson, University of California Radiation Laboratory Report UCRL-3493, 1956 (unpublished).

[45] Bruce M. Foreman, Jr., Walter M. Gibson, Richard A. Glass, and Glenn T. Seaborg, Phys. Rev. **116**, 382 (1959).

Smooth curves are drawn through the measured spallation cross sections for Th^{232}, U^{238}, and U^{233} in Figs. 7–9. We have taken average values of any of the spallation cross sections measured more than once. It should be noted that $\sigma(d,3n)$, $\sigma(d,\alpha n)$, and $\sigma(d,t)$ cross sections are missing for Th^{232}; $\sigma(d,n)$, $\sigma(d,3n)$, and $\sigma(d,\alpha n)$ cross sections are missing for U^{238}; and $\sigma(d,p)$, $\sigma(d,4n)$, and $\sigma(d,t)$ cross sections are missing for U^{233}. However, it is possible to make a reasonable estimate of these missing reaction cross sections. The (d,n), (d,p), (d,t), and $(d,\alpha n)$ processes are known to proceed mostly through direct interaction and therefore it is reasonable to expect that for these heavy elements the reaction cross sections in question should not vary much from element to element. Accordingly, we have assumed the missing (d,p) and (d,t) cross sections for U^{233} to be equal to the known (d,p) and (d,t) cross sections for U^{238}.

It is interesting to note that cross sections for the (d,p) process with Th^{232} and U^{238} are very nearly equal. The cross sections for $(d,\alpha n)$ processes in heavy elements are extremely small compared to the total reaction cross sections. Measurements by Gibson[44] and by Foreman, *et al.*[45] for U^{233} show that $\sigma(d,\alpha n)$ is only about 2 mb at 24-MeV energy and much less at lower deuteron energies. We have therefore neglected the missing $(d,\alpha n)$ cross sections in the case of Th^{232} and U^{238}. Wade *et al.*[46] have measured (d,t) cross sections of Th^{232} and U^{238} by counting tritons, which neglects cross sections for processes such as $(d,p2n)$. We are interested in summing all spallation cross sections and for the (d,t) process take, therefore, only radiochemical measurements which include cross sections such as $(d,p2n)$. However, the $\sigma(d,t)$ measurements of Wade *et al.*[46] do show that these cross sections are equal for Th^{232} and U^{238} although the peaks in the excitation functions for these elements are displaced by about 2 MeV. As a consequence we have assumed the same values of $\sigma(d,p2n)$ for Th^{232} as known from radiochemical measurements of Wing *et al.*[43] for U^{238}, but the $(d,p2n)$ excitation function for Th^{232} has been displaced with respect to that of U^{238} by 2 MeV, as suggested by the (d,t) cross section results of Wade.

The (d,n) process also proceeds through direct interaction. The (d,n) cross sections have been measured[42,44,45] for both Th^{232} and U^{233}. The peak value of $\sigma(d,n)$ is about 44 mb for Th^{232} and 13 mb for U^{233}. These cross sections are quite small compared to the total reaction cross sections, and thus for U^{238} we have assumed an average of the Th^{232} and U^{233} measured (d,n) values. The rest of the missing cross sections are $\sigma(d,3n)$ for Th^{232} and U^{238} and $\sigma(d,4n)$ for U^{233}. Wing *et al.*[43] have shown that their experimental data on $U^{238}(d,2n)$, $U^{238}(d,4n)$, $U^{235}(d,2n)$, and $U^{235}(d,3n)$ excitation functions can be very well fitted by theoretical calculations based on the Jackson model modified for fission. We have therefore calculated the $\sigma(d,3n)$ cross sections of Th^{232} and U^{238} by the method of Wing *et al.*,[43] using nuclear temperature $T=1.35$ MeV. The $(d,4n)$ cross sections for U^{233} calculated by the above method turned out to be very small below 21-MeV deuteron energy, and therefore it has been neglected in calculating the total-reaction cross sections for U^{233}.

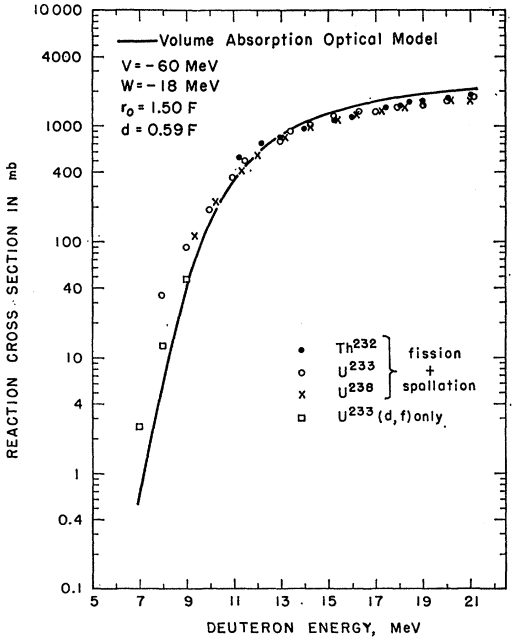

FIG. 14. Comparison of theoretical total reaction cross sections calculated with volume absorption-optical model, with experimentally determined reaction cross sections for heavy elements as a function of deuteron energy in the laboratory system. The fission cross sections for all the points between 7 and 11 MeV were measured with deuterons accelerated with the tandem Van de Graaff. The spallation cross sections were determined, however, with cyclotron accelerated deuterons. The open squares represent fission cross sections for the $U^{233}(d,f)$ reactions and these points are lower limits to the reaction cross section.

Optical-model parameters from an analysis of deuteron elastic scattering on thorium and uranium targets are not available presently. Melkanoff *et al.*,[26,27] however, have analyzed the elastic scattering of deuterons in our energy range for several targets ranging in mass up to lead. Their analysis was carried out with a volume-absorption potential including a real spin-orbit coupling of the Thomas form and characterized by the usual five parameters V, W, V_{SO}, a, and r_0. The solid line in Fig. 14 represents cross sections calculated by means of a volume absorption-optical model with Melkanoff's parameters[27] for gold, $V=-60$ MeV, $W=-18$ MeV, $V_{SO}=-4$ MeV, $a=0.59$ F and $r_0=1.50$ F. The use of these parameters for the Th-U region neglects their dependence on mass number, although the mass dependence of the Woods-Saxon parameters derived from analyses of deuteron elastic-scattering data is very weak.[27] Furthermore, the gold data indicate that the parameters are quite insensitive to

[46] William H. Wade, José Gonzalez-Vidal, Richard A. Glass, and Glenn T. Seaborg, Phys. Rev. **107**, 1311 (1957).

TABLE III. Reaction cross sections calculated with a volume-absorption potential for 9-MeV (laboratory) deuterons on U^{235}. The parameters for calculation No. 1 are those of Melkanoff *et al.* (Ref. 27) for gold.

Calculation	V (MeV)	W (MeV)	r_0 (F)	a (F)	σ_R (mb)
No. 1	−60	−18	1.50	0.59	38.6
No. 2	−52.7	−18	1.50	0.59	35.7
No. 3	−60	−18	1.60	0.59	81.8
No. 4	−60	−18	1.50	0.62	45.3
No. 5	−60	−12	1.50	0.59	37.3
No. 6	−52.7	−18	1.60	0.59	76.0

deuteron energy over the energy range 11 to 24 MeV. Hence, we have neglected any energy dependence in the Woods-Saxon parameters in computing the solid line of Fig. 14.

The curves in the figures show that the calculated cross sections are larger than the experimentally evaluated cross sections at the higher energies. For each target the optical-model cross sections exceed the evaluated total reaction cross sections by an amount of the order of 100 to 300 mb in the energy range 15 to 21 MeV. Since the deuteron binding energy is very small, the possibility of an appreciable cross section for deuteron break-up[47–49]should not be overlooked. The optical-model analyses of elastic scattering reflect deuteron break-up since this process depletes the initial deuteron beam intensity, and hence, resembles a real nuclear reaction. Due to the lack of measurements of this cross section in the literature, it was not possible to add values of the cross section of the deuteron break-up process to the spallation cross sections. We conclude that the observed difference between the evaluated and optical-model values of the total-reaction cross section may be due largely, if not entirely, to deuteron break-up.

The spallation cross sections measured with the lower energy deuterons accelerated by the Argonne fixed frequency cyclotron are subject to large errors due both to the large uncertainty in beam energy and large energy dispersion following energy degradation by absorbers. Hence, at deuteron energies of 7 to 9 MeV the fission cross sections measured with the tandem Van de Graaff for our most fissionable target U^{233} are also plotted in Fig. 14. These values represent lower limits to the deuteron reaction cross sections. Over the energy interval 7 to 9 MeV, the fission cross sections alone are larger than the reaction cross sections calculated with a volume-absorption optical model with parameters $V=-60$ MeV, $W=-18$ MeV, $r_0=1.50$ F, and $a=0.59$ F. The computed reaction cross sections for 9-MeV deuterons on U^{235} for a variety of Woods-Saxon parameters are listed in Table III. The parameters[27] of calculation No. 1 give the reaction cross section plotted in Fig. 14. From calculations 2, 3, 4, and 5 in which a single parameter V, r_0, a, and W is varied respectively, one observes only small changes in the reaction cross sections for all calculations except No. 3 in which the radius parameter is varied. The value of Vr_0^2 in calculation No. 6 was kept equal to that of calculation No. 1 since this is the quantity fixed by analyses of elastic-scattering data. However, most of the change in reaction cross section is due to the change in the radius parameter. The computed reaction cross sections with the larger value of r_0 give a better fit to the experimental data at the low-deuteron energies. The parameters of calculation No. 6 in Table III would lead also to slightly larger computed reaction cross sections at the higher energies. This would produce a still larger difference between our measured reaction cross sections (fission+spallation) and the optical-model predictions. Such a result is compatible with our present lack of knowledge about the magnitude of the deuteron break-up cross section.

The radius parameter used in the optical-model calculations (see Table III) is an interaction radius. For the system $U^{235}+d$, a radius parameter of $r_0=1.50$ F gives an interaction radius of 9.257 F where the absolute value of the potential has dropped by a factor of 2. This is equivalent to a radius of 7.714 F for U^{235} ($r_0=1.25$) and a deuteron radius of 1.543 F. The absolute value of the potential has decreased a factor of 10 at an interaction radius of 10.55 F.

ACKNOWLEDGMENTS

The authors wish to thank members of the cyclotron group for operation of the cyclotron, and members of the Tandem Van de Graaff group for operation of the Van de Graaff accelerator. We are indebted to T. H. Braid and J. T. Heinrich for use of their 18-in.-scattering chamber and wish to thank R. Vandenbosch for helpful discussions. One of us (R. Chaudhry) wishes to thank the International Cooperation Administration, Washington, the International Institute of Nuclear Science and Engineering of the Argonne National Laboratory, and the U. S. Atomic Energy Commission for providing opportunity to work at the Argonne National Laboratory.

[47] L. Landau and E. Lifshitz, Zh. Eksperim. i Teor. Fiz. **18**, 750 (1948).
[48] C. J. Mullin and E. Guth, Phys. Rev. **82**, 141 (1951).
[49] E. W. Hamburger, B. L. Cohen, and R. E. Price, Phys. Rev. **121**, 1143 (1961).